Journal of Applied Research in Optics and Laser Technology,Volume 1, Number 7, Summer 2026

Numerical modeling of laser-induced thermal damage in skin: comparison of a coupled local thermal non-equilibrium–dual-phase-lag model with the Pennes model

Fahimeh Hamzavi[1], Mohammad Javad Karimi[1]*, Mahdi Bahadoran[1]

[1]*Department of Physics, Shiraz University of Technology, Shiraz, Iran*

Received: 2026-07-01 Final revised: 2026-08-12 Accepted: 2026-09-10

Abstract

Heat transfer in biological tissues under laser irradiation plays a crucial role in improving the efficiency and safety of photothermal therapies; therefore, selecting an appropriate model for predicting tissue thermal responses is essential. The thermal response and thermal damage in skin tissue exposed to two laser beams were numerically investigated using a coupled model combining the local thermal non-equilibrium (LTNE) model and the dual-phase-lag (DPL) model, and the results were compared with the Pennes formulation. The governing equations were solved using the finite difference method implemented in MATLAB, and the effects of laser irradiation intensity and pulse timing parameters on the temperature distribution and thermal damage were examined. Compared with the Pennes model, the local thermal non-equilibrium model coupled with the dual-phase-lag model predicted higher temperatures and greater thermal damage. When validated against experimental measurements, the local thermal non-equilibrium model coupled with the dual-phase-lag model reduced the temperature discrepancy from approximately 1.7 °C, as obtained using the Pennes bioheat model, to approximately 0.5 °C, demonstrating closer agreement with the experimental data.

Keywords: Bioheat transfer, Local thermal non-equilibrium, Dual-phase-lag, Laser, Thermal damage.

* Corresponding Author: karimi@sutech.ac.ir

1. Introduction

With advancements in energy-based technologies such as lasers, microwaves, and ultrasound, thermal therapies have become effective treatments for various conditions, including skin cancer, skin lesions, and tissue repair. These therapies rely on the controlled delivery of thermal energy to ablate target tissue while minimizing damage to surrounding healthy tissue. Accordingly, accurate prediction of heat transfer and temperature distribution in biological tissues is essential for optimizing treatment efficacy and safety [1].

As the largest organ of the human body, the skin plays an important role not only in providing protection but also in regulating body temperature, exchanging heat with the surrounding environment, and maintaining physiological homeostasis. Heat transfer in the skin is a complex process governed not only by thermal conduction but also by factors such as tissue perfusion, metabolic heat generation, and the multilayered and heterogeneous structure of the tissue. These characteristics have made accurate modeling of the thermal response of the skin an important research topic in biomedical engineering and energy-based therapies [2]. Among the various heat sources, lasers have gained a prominent position in medical treatments owing to their high precision, ability to concentrate energy, and minimal collateral damage. In addition to therapeutic applications, lasers are used in diagnostic techniques, such as laser Doppler imaging, as well as to accelerate wound healing [3]. The thermal response of biological tissue to laser irradiation depends not only on the temporal characteristics of the irradiation but also on the spatial characteristics of the laser beam. Among the various beam profiles, Gaussian beams are widely used in laser treatments. With their bell-shaped intensity distribution, Gaussian beams concentrate energy in the central region and are highly suitable for applications such as tumor ablation, microsurgery, and photothermal therapy [4]. Various bioheat transfer models have been developed to analyze the thermal response of biological tissues. The classical Pennes model, which is based on Fourier's law of heat conduction, remains one of the most widely used bioheat transfer models because of its simplicity and limited number of required parameters. However, under conditions involving rapid heating, continuous laser irradiation, and heterogeneous tissues, this model may not accurately describe the actual behavior of heat transfer. Consequently, non-Fourier models, such as the single-phase-lag (SPL) and dual-phase-lag (DPL) models, have been developed to account for the effects of the relaxation times associated with heat flux and temperature gradients in heat transfer processes [5]. On the other hand, the local thermal non-equilibrium (LTNE) model, which considers independent temperatures for the tissue and blood phases, provides a more realistic description of heat transfer in biological porous media and offers greater accuracy in predicting tissue thermal responses than models based on thermal equilibrium.

Numerous studies have investigated heat transfer in biological tissues subjected to laser irradiation. Zhang et al. [6] investigated the thermal response of biological tissues exposed to Gaussian laser irradiation using a computational model. Their results showed that the energy generated by Gaussian beams leads to highly localized heating, which is essential for applications such as tumor ablation and photothermal therapy. Jiang et al. [7] investigated the effects of laser wavelength and spot size on burn severity and highlighted laser irradiation conditions that minimize tissue damage. Wang et al. [8] employed a nonlinear DPL model to investigate heat transfer in multilayer skin subjected to short-pulse laser irradiation and analyzed the effects of physical parameters on the

thermal response and tissue damage. In the field of heat transfer modeling, recent studies have focused on developing advanced models, such as LTNE and DPL. Dinda et al. [9] used the LTNE model to analyze the coupling between laser energy transfer and thermal dose in cancer treatment. Jasiński et al. [10] employed a numerical analysis based on a generalized DPL equation to investigate soft tissue subjected to laser irradiation. They considered internal heat generation induced by laser irradiation, investigated tissue damage, and presented results for different porosities.

Despite significant advances in bioheat transfer modeling, most previous studies have considered only some aspects of the actual behavior of biological tissues. The combined effects of the porous structure of the skin, thermal non-equilibrium between blood and tissue, non-Fourier heat transfer behavior, and the spatial and temporal characteristics of laser irradiation have not yet been comprehensively investigated. Therefore, in the present study, a bioheat transfer model based on the coupling of the LTNE and DPL models is developed to simulate the thermal response of the skin under simultaneous irradiation by two continuous-wave Gaussian laser beams, and its performance is compared with that of the classical Pennes model. Accordingly, the temporal and spatial variations in temperature, temperature distributions, and thermal damage in the tissue are investigated, and the effects of laser intensity and pulse timing on the thermal behavior of the tissue are analyzed. This study demonstrates that the proposed model can provide more accurate predictions of tissue thermal responses by accounting for thermal non-equilibrium between blood and tissue and the effects of thermal relaxation, thereby serving as a useful tool for optimizing laser-based photothermal treatments.

2 .Theory and Methodology

2.1 Theoretical Background

In this study, the skin tissue is modeled as a biological porous medium consisting of two distinct phases: the vascular phase (blood) and the extravascular phase (tissue). The vascular phase is responsible for heat transfer and transport through blood flow, while the extravascular phase is where laser energy is absorbed. As shown in Fig. 1, a biological tissue with a high absorption coefficient and a thickness of (H) is considered to investigate the thermal response of the tissue under irradiation by two laser beams at different locations. A schematic of the problem geometry and the laser irradiation configuration is presented in Fig. 1.

The Pennes bioheat equation, widely used for heat transfer in living tissues, predicts temperature distribution by incorporating thermal conduction, blood perfusion, metabolic heat, and external heat sources. It forms the basis of many advanced models and is expressed as [11]:

$$\rho c_b \frac{\partial T}{\partial t} = \nabla\left(k\nabla T\right) + \rho_b w_b c_b \left(T\right) + Q_m + Q_L \tag{1}$$

where ρ is the tissue density, c_b is the specific heat capacity of the tissue, T is the tissue temperature, k is the tissue thermal conductivity, ρ_b is the blood density, w_b is the tissue blood perfusion rate, Q_m is the metabolic heat generation, and Q_L is the heat generated by the laser source. In this study, the LTNE model coupled with the DPL model is employed to provide a more accurate description of the thermal behavior of the tissue.

The governing heat transfer equations for the LTNE model in a two-dimensional, single-layer tissue, accounting for porosity, dual-phase-lag effects, heat exchange between blood and tissue, tissue blood perfusion, and the heat source induced by laser irradiation, are expressed as follows [8]:

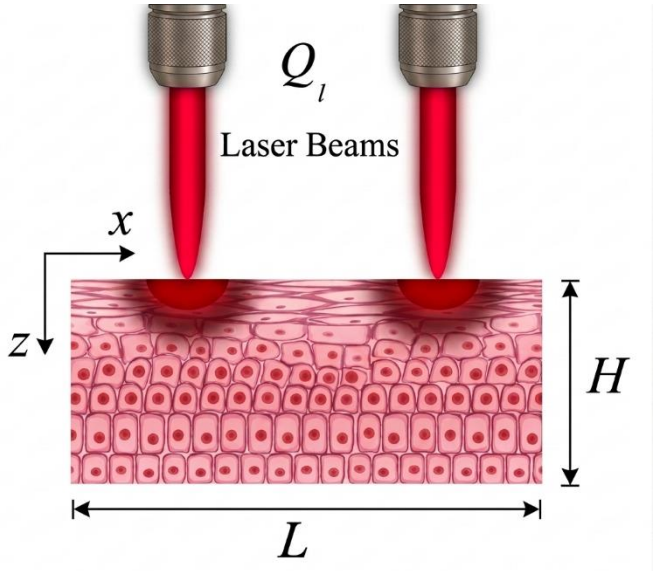


Fig. 1. Schematic of skin tissue under irradiation by two laser beams.

For the blood phase:

$$\varepsilon(\rho c)_b\left(\frac{\partial T_b}{\partial t}+V\cdot\nabla T_b\right)=\varepsilon k_b\left(\nabla^2 T_b\right)+\alpha\mathrm{A}\left(T_t-T_b\right)+wc_b\left(T_t-T_b\right)+\varepsilon Q_{mb}+\varepsilon Q_L \tag{2}$$

For the tissue phase:

$$\left(1-\varepsilon\right)(\rho c)_t\frac{\partial T_t}{\partial t}=\left(1-\varepsilon\right)k_t\left(\nabla^2 T_t\right)+\alpha\mathrm{A}\left(T_t-T_b\right)-wc_b\left(T_t-T_b\right)+\left(1-\varepsilon\right)Q_{mt}+\left(1-\varepsilon\right)Q_L \tag{3}$$

where ε is the tissue porosity, V is the blood velocity, α is the heat transfer coefficient and A is the interfacial heat transfer coefficient between the tissue and blood. The subscripts t and b denote the tissue and blood phases, respectively. In this model, the blood temperature and tissue temperature are treated as independent variables and are coupled through the interfacial heat transfer coefficient between the two phases. This relationship is expressed as follows:

$$\varepsilon(\rho c)_b\frac{\partial T_b}{\partial t}=\alpha\mathrm{A}\left(T_t-T_b\right)+wc_b\left(T_t-T_b\right) \tag{4}$$

By adding Eqs. (2), (3) and applying the relationship given in Eq. (4), the governing equation is obtained as follows:

$$\frac{\partial T_b}{\partial t}+\tau_q\frac{\partial^2 T_b}{\partial t^2}+\frac{\varepsilon\rho_b c_b}{(\rho c)_{eff}}(V\cdot\nabla\mathrm{T}_t)=\alpha_{eff}\left(\nabla^2 T_b+\tau_T\frac{\partial}{\partial t}\left(\nabla^2 T_b\right)\right)+\frac{\varepsilon Q_{mb}+(1-\varepsilon)Q_{mt}+Q_L}{(\rho c)_{eff}} \tag{5}$$

where

$$\left(\rho c\right)_{eff}=\varepsilon(\rho c)_b+\left(1-\varepsilon\right)(\rho c)_t \tag{6}$$

$$\alpha_{eff}=\frac{k_{eff}}{\left(\rho c\right)_{eff}} \tag{7}$$

$$k_{eff} = \varepsilon\, k_b + (1-\varepsilon) k_t \tag{8}$$

$$\tau_q = \frac{\varepsilon(\rho c)_b + (1-\varepsilon)(\rho c)_t}{G\,(\rho c)_{eff}} \tag{9}$$

$$\tau_T = \frac{\varepsilon(\rho c)_b + (1-\varepsilon)(\rho c)_t k_b}{G\; k_{eff}} \tag{10}$$

where T_t is the tissue temperature, T_b is the blood temperature, $(\rho c)_{eff}$ is the effective volumetric heat capacity, k_{eff} is the effective thermal conductivity, α_{eff} is the effective heat transfer coefficient, τ_q is the heat-flux relaxation time, τ_T is the temperature-gradient relaxation time, and G is the blood–tissue coupling coefficient. In this study, $\tau_q = 0.478(s)$, $\tau_T = 0.478(s)$, $G = 34954\left(W/m^3K\right)$ and $\varepsilon = 0.0041$ [5].

The governing equation for the tissue temperature is obtained by substituting Eq. (4) into Eq. (5), as follows:

$$\begin{aligned}&\frac{\partial T_t}{\partial t} + \tau_q \frac{\partial^2 T_t}{\partial t^2} + \frac{\varepsilon\rho_b c_b}{(\rho c)_{eff}}(V\cdot\nabla \mathrm{T}_t) + \frac{\varepsilon^2\rho_b{}^2 c_b{}^2}{G\,(\rho c)_{eff}}\left(\frac{\partial V}{\partial t}\cdot(\nabla T_b)\right) = \alpha_{eff}\left(\nabla^2 T_t + \tau_T \frac{\partial}{\partial t}(\nabla^2 T_t)\right)\\ &+\frac{\varepsilon Q_{mb} + (1-\varepsilon)Q_{mt} + Q_L}{(\rho c)_{eff}} + \frac{\varepsilon(\rho c)_b}{G\,(\rho c)_{eff}}\left(\varepsilon\frac{\partial Q_{mb}}{\partial t} + (1-\varepsilon)\frac{\partial Q_{mt}}{\partial t} + \frac{\partial Q_L}{\partial t}\right)\end{aligned} \tag{11}$$

Assuming that the approximation $\frac{\partial V}{\partial t} \approx 0$ holds, and also considering $-\varepsilon\rho_b c_b V\cdot\nabla \mathrm{T}_t \approx G(T_b - T_t)$ and the two-dimensional nature of the problem, Eq. (11) is reduced to the following form:

$$\begin{aligned}&\frac{\partial T_t}{\partial t} + \tau_q \frac{\partial^2 T_t}{\partial t^2} - \frac{G}{(\rho c)_{eff}}(T_b - T_t) = \alpha_{eff}\left(\frac{\partial^2 T_t}{\partial x^2} + \frac{\partial^2 T_t}{\partial z^2} + \tau_T\left(\frac{\partial^3 T_t}{\partial t\,\partial x^2} + \frac{\partial^3 T_t}{\partial t\,\partial z^2}\right)\right)\\ &+\frac{\varepsilon Q_{mb} + (1-\varepsilon)Q_{mt} + Q_L}{(\rho c)_{eff}} + \frac{\varepsilon(\rho c)_{eff}}{G\,(\rho c)_{eff}}\left(\varepsilon\frac{\partial Q_{mb}}{\partial t} + (1-\varepsilon)\frac{\partial Q_{mt}}{\partial t} + \frac{\partial Q_L}{\partial t}\right)\end{aligned} \tag{12}$$

In this study, the laser energy distribution is modeled as a Gaussian beam. For a Gaussian beam, the irradiation intensity reaches its maximum at the beam center and decreases exponentially with increasing distance from the central axis, thereby producing a nonuniform temperature distribution within the tissue. Considering two laser beams irradiating the tissue simultaneously over specified time intervals, the laser heat source is defined as follows [5]:

$$Q_L(x,z,t) = I_1(t)\Phi(x,z) + I_2(t)\Phi(x,z) \tag{13}$$

In these equations, I_1 and I_2 are the temporal functions of the laser beams, defined as follows:

$$\begin{aligned}\mathrm{I}_1(t) &= \begin{cases} 1 & t_1 \le t \le t_2 \\ 0 & otherwise \end{cases}\\ \mathrm{I}_2(t) &= \begin{cases} 1 & t_3 \le t \le t_4 \\ 0 & otherwise \end{cases}\end{aligned} \tag{14}$$

where t_1, t_2, t_3 and t_4 are equal to 0, 30, 150, and 180 s, respectively. The energy distribution for a Gaussian beam is expressed using the Beer–Lambert law as follows [5]:

$$\Phi(x,z)=(1-R_d)\mu_a Q\left(e^{\frac{-2(x-x_0)^2}{\sigma^2}}+e^{\frac{-2(x-x_1)^2}{\sigma^2}}\right)e^{-\mu_t z} \tag{15}$$

where R_d is the skin surface reflectance, μ_a is the absorption coefficient, Q is the laser intensity, σ is the laser beam radius, and μ_t is the attenuation coefficient. The total tissue attenuation coefficient is defined as follows [12]:

$$\mu_t = \mu_a + \mu_s \tag{16}$$

where μ_a and μ_s are the tissue absorption and scattering coefficients, respectively. The optical penetration depth is also defined as the reciprocal of the attenuation coefficient [12]:

$$L_p = \frac{1}{\mu_t} \tag{17}$$

The optical penetration depth depends on the laser wavelength because the absorption and scattering properties of tissue are wavelength-dependent. In the present study, a pulsed Nd:YAG laser with a wavelength of 1064 nm is used as the heat source. This wavelength lies in the near-infrared region and is selected because of its suitable penetration into biological tissues and its widespread use in laser therapy studies. Accordingly, the optical coefficients corresponding to a wavelength of 1064 nm are used to model radiative energy transport in the tissue [13]. Fig. 2 shows the laser energy distribution for an intensity of $1\times10^6 W/m^2$.

In this study, skin tissue with a thickness of (H) is subjected to laser irradiation. Given the high absorption coefficient of the tissue, the laser energy is applied to the tissue surface as a heat flux. The bottom surface of the tissue is assumed to be thermally insulated, such that no heat flux passes through this boundary. Thermal insulation conditions are also imposed on the lateral boundaries. Accordingly, the model boundary conditions are expressed as follows:

For the x-axis:

$$\begin{aligned}&\frac{\partial T_t}{dx}(0,z,t)=0\\&\frac{\partial T_t}{dx}(L,z,t)=0\end{aligned} \tag{18}$$

For the z-axis:

$$\begin{aligned}&-k_{eff}\,\frac{\partial T_t}{\partial z}(x,0,t)=\Phi(x,0,t)\\&\frac{\partial T_t}{\partial z}(x,H,t)=0\end{aligned} \tag{19}$$

Furthermore, at the beginning of the process, the tissue and blood are assumed to be in thermal equilibrium, with the temperatures of both phases throughout the domain equal to the initial body temperature. Accordingly, the initial conditions of the model are defined as follows:

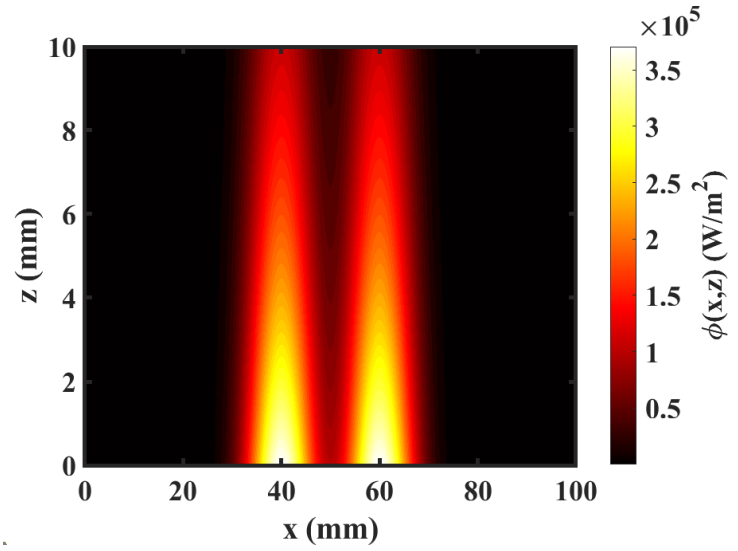


Fig. 2. Laser energy distribution for a Gaussian beam.

$$T_t\left(x,z,0\right)=T_{t_0}$$
$$\frac{\partial T_t}{\partial x}(x,z,0)=0 \tag{20}$$
$$T_b\left(x,z,0\right)=T_{b_0}$$

The Arrhenius model is used to evaluate thermal damage caused by temperature elevation and is expressed as follows [14]:

$$\alpha=\int_0^t A\ \exp(-\frac{E_a}{RT})dt \tag{21}$$

In this equation, α represents the degree of tissue damage, $A=3.1\times10^{98}s^{-1}$ is the frequency factor, T is the absolute temperature, $E_a=6.27\times10^5\left(J/_{mol}\right)$ is the activation energy, and R is the universal gas constant, equal to $8.318\left(J/_{mol.K}\right)$ [14].

2.2 Numerical Model

The governing heat transfer equations, together with the initial and boundary conditions, were solved in MATLAB using the finite difference method (FDM). In all simulations, the thermophysical properties of blood and tissue, as well as the laser parameters, are presented in Tables 1 and 2. To investigate the effect of each parameter, only that parameter was varied, while all other model parameters were kept constant. To achieve adequate temporal accuracy, a time step of 0.001 s was used in all numerical simulations. Furthermore, to examine the independence of the results from the computational mesh, simulations were performed using meshes with different numbers of grid points. As shown in Table 3, increasing the number of grid points resulted in negligible changes in the maximum temperature, with differences between the results remaining below 0.1°C. Therefore, a 201×201 mesh was selected as an appropriate mesh for the simulations.

Table 1. Thermophysical properties of blood and tissue [5,8].

Parameter	Tissue	Blood
Specific heat capacity $\left(J/kg.K\right)$	4187	3860
Thermal conductivity $\left(W/m.K\right)$	0.628	0.5
Density $\left(kg/m^3\right)$	1000	1060
Initial temperature $\left(^\circ C\right)$	37	37

Table 2. Laser beam parameter values [5].

Parameter	Value
Laser absorption coefficient $\mu_a\left(m^{-1}\right)$	0.4
Laser light reflectance R_d	0.05
Laser scattering coefficient $\mu_s\left(m^{-1}\right)$	120
Laser beam width $\sigma\left(m\right)$	1.0

3 . Results and Discussion

Initially, the numerical model was validated by comparing the simulation results obtained using the LTNE+DPL model with those reported in the reference study [8]. Fig. 3 shows the temperature variation over time under the same conditions as those used in the reference study. The good agreement between the present results and the reference data confirms the correct implementation of the numerical model and solution method.

Table 3. Independence of the maximum temperature from the number of grid points.

Nx	Nz	$T_{max,LTNE+DPL}$ $(℃)$	$T_{max,Pennes}$ $(℃)$
51	51	43.25	42.92
101	101	43.26	42.94
201	101	43.26	42.93
101	201	43.28	42.95
201	201	43.28	42.95
501	501	43.29	42.96

Furthermore, in Fig. 4, the simulation results obtained using the Pennes and LTNE+DPL models in the present study are compared with those reported by Shi et al. [15]. In the reference study, ex vivo porcine skin was exposed to laser irradiation at a wavelength of 1064 nm for 30 s, and the experimentally measured thermal response was compared with the simulation results obtained using the Pennes model in COMSOL

Multiphysics. As shown in Fig. 4, the Pennes model implemented in the present study reproduces the simulation results of the reference study well. However, at the end of the 30-s irradiation period, the experimentally measured temperature was 43.1 °C, whereas the temperatures predicted by the Pennes and LTNE+DPL models were approximately 41.4 °C and 42.6 °C, respectively. Therefore, the discrepancy between the predicted and experimental temperatures decreases from approximately 1.7 °C for the Pennes model to 0.5 °C for the LTNE+DPL model. These results indicate that the LTNE+DPL model provides better agreement with the experimental data under the conditions investigated.

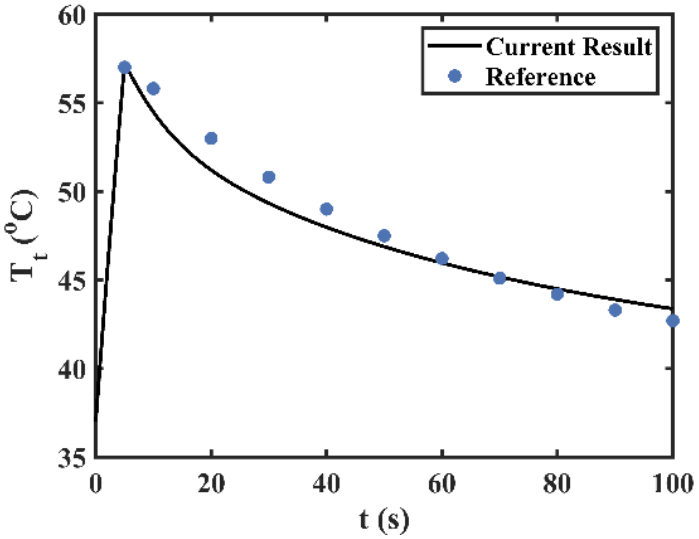


Fig. 3. Validation of the model results against the reference results [8] for $t_1 = 5s$ and $Q = 3^{W}/_{cm^2}$

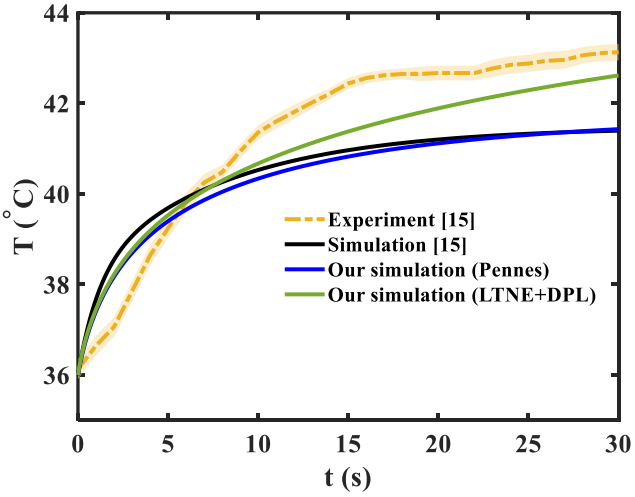


Fig. 4. Validation of the model results against the experimental data and simulation results reported in the reference study [15].

The numerical simulation results obtained using the LTNE+DPL model are presented and compared with those of the classical Pennes model for tissue heating under irradiation by two Gaussian laser beams. In all simulations, the horizontal positions of the two laser beams were fixed at $x_0 = 4\,mm$ and $x_1 = 6\,mm$, respectively, and the thermal response

and tissue damage were investigated after 400 s of irradiation. To evaluate the performance of the models, the temporal variations in temperature and the temperature profiles along the depth and horizontal directions, as well as the temperature distributions and tissue damage parameter, were analyzed for different laser intensities and pulse timing schemes.

The transient tissue temperatures predicted by the LTNE+DPL model and compared with the Pennes model at two laser intensities are shown in Fig. 5. In both models, temperature rises sharply during each pulse and decays after pulse-off due to heat diffusion and dissipation, with higher intensities yielding higher peak temperatures. The LTNE+DPL model consistently predicts higher temperatures than the Pennes model, attributable to local thermal non-equilibrium between blood and tissue and the phase-lag effects in heat propagation.

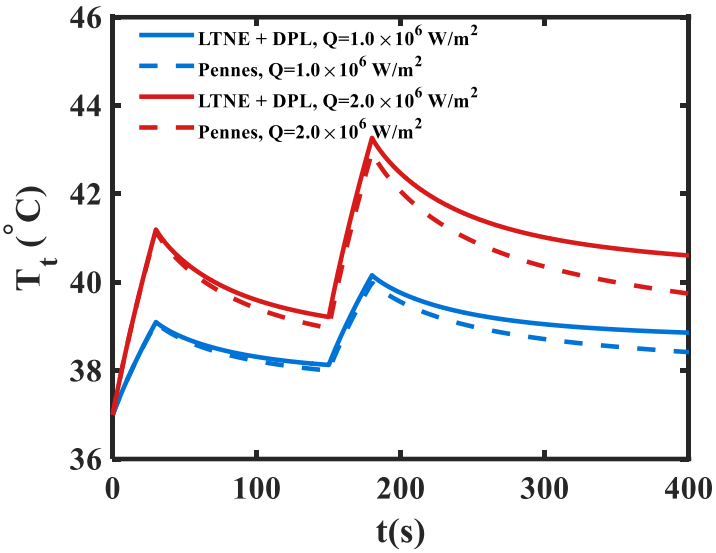


Fig. 5. Temporal variations in tissue temperature predicted by the Pennes and LTNE+DPL models at two different laser intensities**.**

Fig. 6 illustrates the temperature variation with tissue depth at two laser intensities. Maximum temperature occurs at the irradiated surface and decreases with depth due to attenuation of absorbed laser energy, while higher intensities elevate temperatures at all depths. The LTNE+DPL model predicts higher temperatures than the Pennes model across the tissue thickness, with the discrepancy most pronounced near the irradiated surface where energy absorption is highest.

Fig. 7 shows the temperature distribution along the horizontal direction of the tissue for two different laser intensities. As observed, the use of two laser beams results in two temperature peaks at the beam irradiation locations. As the distance from these regions increases, the temperature gradually decreases and approaches the initial tissue temperature. Furthermore, increasing the laser intensity leads to higher temperature peaks in both models.

Fig. 8 compares the x–z temperature contours predicted by the LTNE+DPL and Pennes models at two laser intensities. In both models, peak temperatures occur at the irradiation spots and decay with distance and depth. Higher intensity increases both the maximum temperature and the extent of the heated zone. The LTNE+DPL model yields

higher temperatures and a larger heated region than the Pennes model, owing to local thermal non-equilibrium and phase-lag effects in heat transfer.

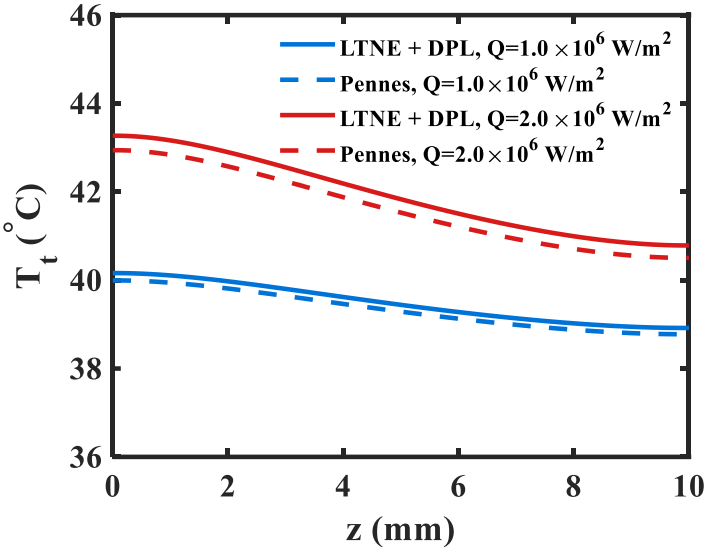


Fig. 6. Temperature variations as a function of tissue depth for two different laser intensities predicted by the Pennes and LTNE+DPL models.

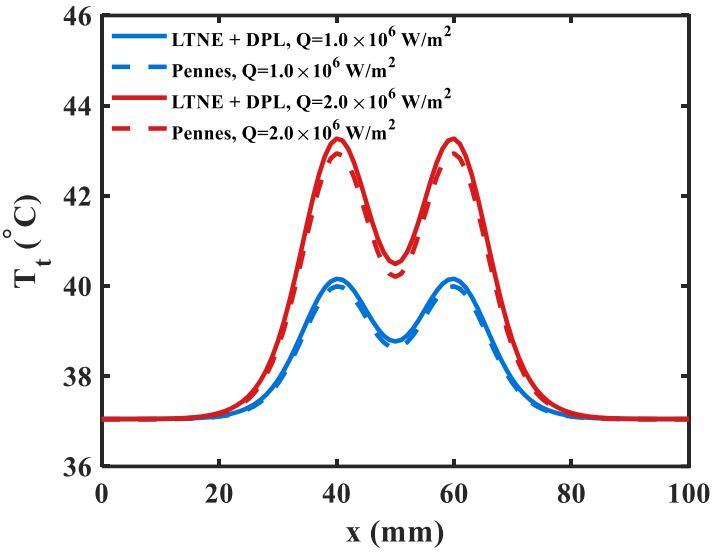


Fig. 7. Temperature distribution along the horizontal direction of the tissue for two different laser intensities: comparison of the Pennes and LTNE+DPL models.

Fig. 9 shows the variations in the tissue damage parameter along the x-axis for two different laser intensities. As observed, the highest damage parameter values occur near the tissue surface and gradually decrease with increasing distance along the x-axis, owing to the attenuation of laser energy absorption within the tissue. Furthermore, increasing the laser intensity leads to a significant increase in the damage parameter throughout the tissue depth. A comparison of the results obtained using the two models indicates that the LTNE+DPL model predicts higher values of the Arrhenius damage parameter than the Pennes model throughout the tissue thickness. This difference results from the higher

temperatures predicted by the LTNE+DPL model, which ultimately lead to increased thermal damage to the tissue.

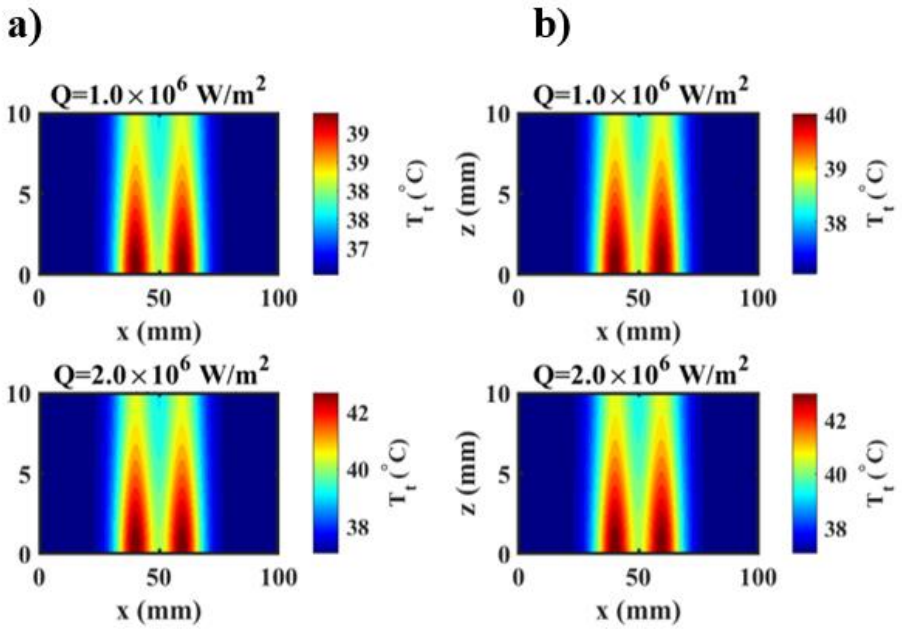


Fig. 8. Comparison of temperature distributions in the x–z plane at two different laser intensities: (a) Pennes model and (b) LTNE+DPL model.

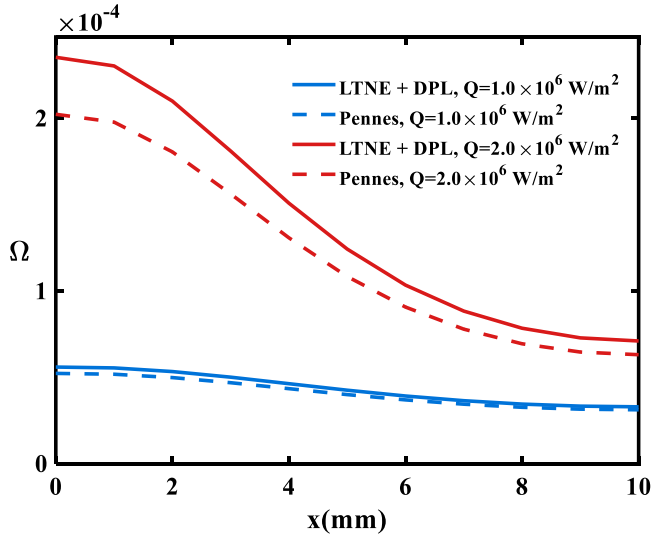


Fig. 9. Comparison of tissue damage parameter variations along the x-axis for the Pennes and LTNE+DPL models at two different laser intensities.

Fig. 10 shows the temporal variations in the tissue damage parameter for two different laser intensities. As observed, the damage parameter increases rapidly during each laser pulse, and its rate of increase decreases after the irradiation ends. Furthermore, increasing the laser intensity leads to greater cumulative tissue damage in both models. A comparison of the results indicates that the LTNE+DPL model predicts higher values of the Arrhenius damage parameter than the Pennes model at all times. In addition, the greatest damage occurs during the period from 150 to 180 s, coinciding with the

application of the second laser pulse, indicating the significant contribution of the second pulse to the enhancement of thermal tissue damage.

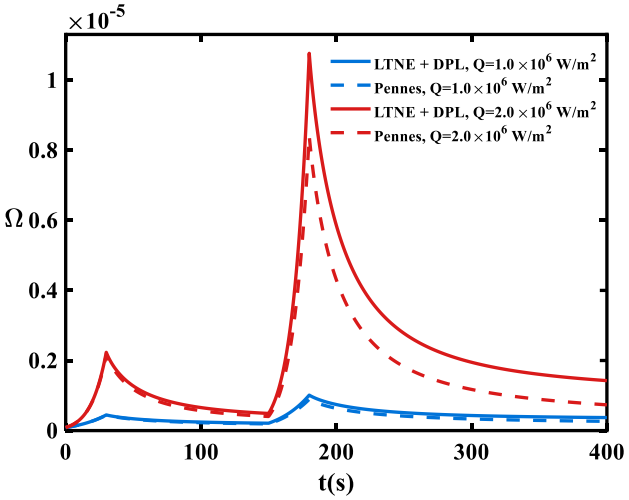


Fig. 10. Comparison of the temporal variations in the tissue damage parameter predicted by the Pennes and LTNE+DPL models at two different laser intensities.

In this section, the effects of laser pulse timing on the thermal response and tissue damage are investigated. To this end, the pulse initiation times are varied while keeping the other laser parameters constant, and their effects on temperature distribution and thermal damage are evaluated using the Pennes and LTNE+DPL models. Fig. 11 shows the temporal variations in tissue temperature for two different laser pulse timing schemes, as predicted by the LTNE+DPL and Pennes models. The results indicate that shifting the application time of the second pulse from 30 to 50 s and that of the fourth pulse from 180 to 200 s increases the maximum tissue temperature and maintains a higher temperature during the post-irradiation phase. This behavior results from changes in the thermal interactions between the pulses and greater heat accumulation within the tissue. Furthermore, the LTNE+DPL model predicts higher temperatures than the Pennes model in both cases.

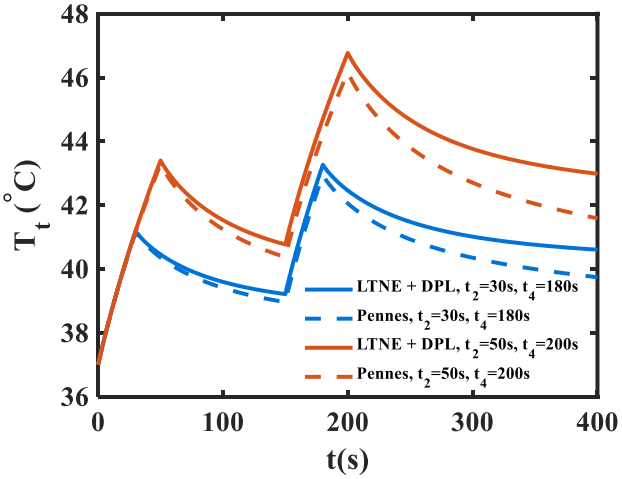


Fig. 11. Temporal variations in tissue temperature for two different laser pulse timing schemes predicted by the Pennes and LTNE+DPL models.

Fig. 12 shows the temperature variations along the tissue depth for two different laser pulse timing schemes. As observed, the temperature gradually decreases with increasing depth in both cases, owing to the attenuation of laser energy absorption within the tissue. Furthermore, changing the laser pulse timing increases the temperature throughout the tissue depth, particularly in the superficial layers. A comparison of the results obtained using the two models indicates that the LTNE+DPL model predicts slightly higher temperatures than the Pennes model throughout the tissue thickness, with this difference being more pronounced in regions close to the irradiated surface.

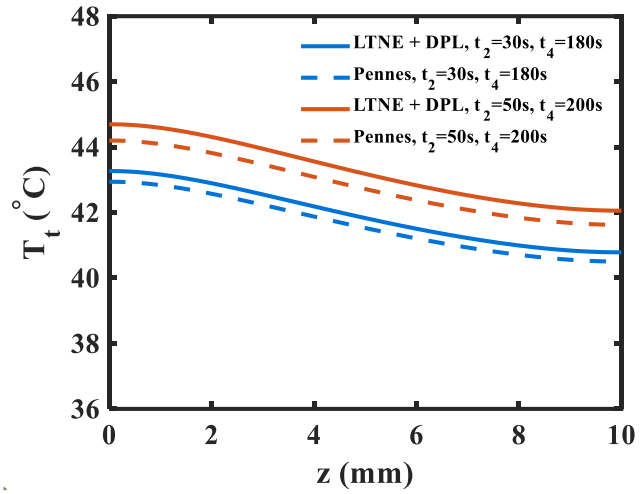


Fig. 12. Temperature distribution along the tissue depth for two different laser pulse timing schemes predicted by the Pennes and LTNE+DPL models.

Fig. 13 shows the temperature distribution along the horizontal direction of the tissue for two different laser pulse timing schemes. As observed, two temperature peaks form at the irradiation locations of the two laser beams in both cases. Changing the laser pulse timing increases the maximum temperature in the irradiated regions, while the overall shape of the temperature distribution remains largely unchanged. Furthermore, the LTNE+DPL model predicts slightly higher temperatures in the heated regions than the Pennes model.

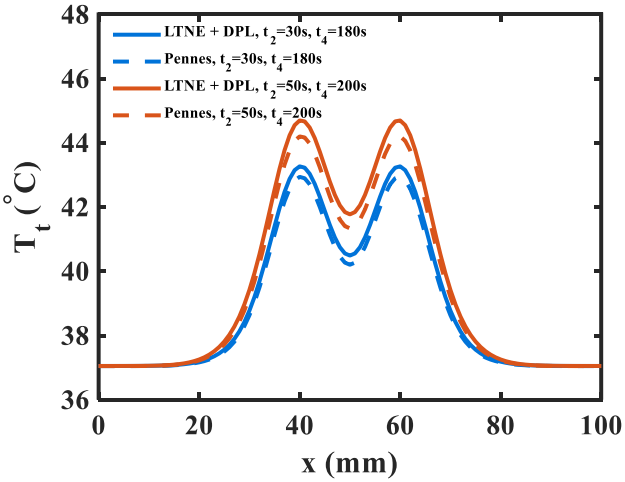


Fig. 13. Temperature distribution along the horizontal direction of the tissue for two different laser pulse timing schemes predicted by the Pennes and LTNE+DPL models.

Fig. 14 shows the temperature distribution for two different laser pulse timing schemes predicted by the LTNE+DPL and Pennes models. As observed, in both models, the highest temperatures are concentrated in the laser-irradiated regions, and the temperature gradually decreases with increasing distance from the irradiation sites and increasing tissue depth. Changing the pulse timing increases the maximum temperature and expands the heated region within the tissue. Thermal penetration into deeper layers also increases, indicating greater heat accumulation in the tissue. Comparison of the results from the two models shows that the LTNE+DPL model predicts a region with higher temperatures and a larger spatial extent than the Pennes model. This difference arises from accounting for local thermal nonequilibrium between blood and tissue, as well as the time-delay effect in heat-flux propagation.

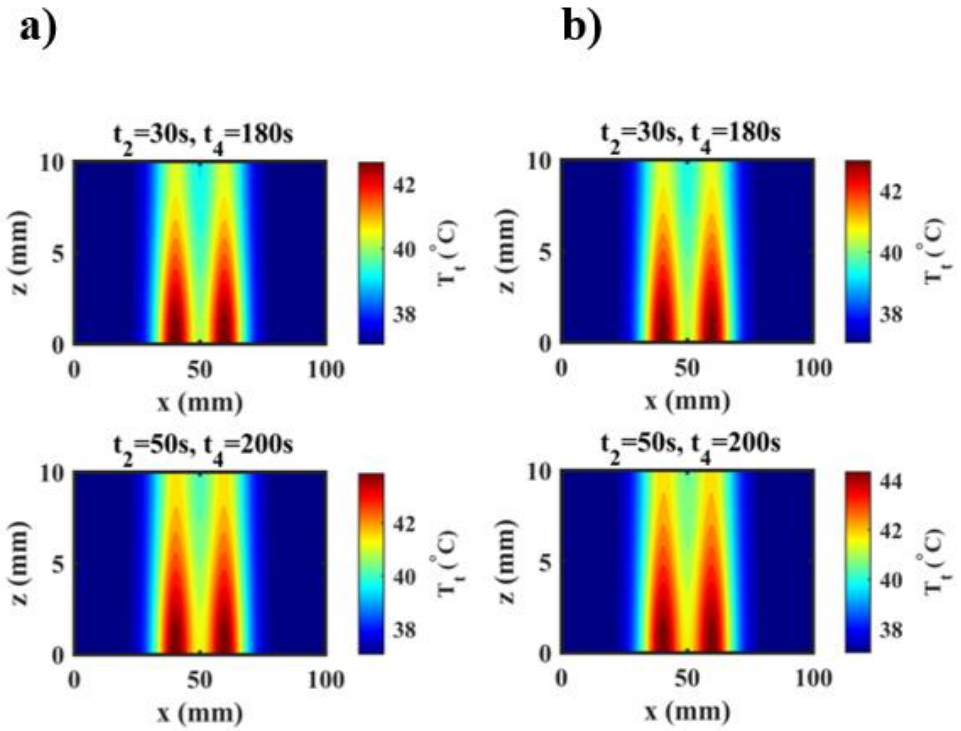


Fig. 14. Temperature distribution in the tissue for two different laser pulse timing schemes: (a) Pennes model and (b) LTNE+DPL model.

Fig. 15 shows the variations in the tissue damage parameter along the x-axis for two different laser pulse timing schemes. As observed, the damage parameter reaches its maximum in regions near the irradiation sites and gradually decreases with increasing distance along the x-axis. Furthermore, changing the laser pulse timing increases the damage parameter throughout the investigated region. Comparison of the results from the two models also indicates that the LTNE+DPL model predicts higher values of the Arrhenius damage parameter than the Pennes model at all locations.

Fig. 16 shows the temporal variations in the Arrhenius damage parameter for two different laser pulse timing schemes. As observed, the damage parameter increases during the application of each pulse, and its rate of increase gradually decreases after irradiation ends. The maximum damage parameter is observed during the application of the second pulse. Furthermore, changing the laser pulse timing leads to a considerable increase in

the damage parameter throughout the heating process. Comparison of the results from the two models also indicates that the LTNE+DPL model predicts higher values of the Arrhenius damage parameter than the Pennes model at all times.

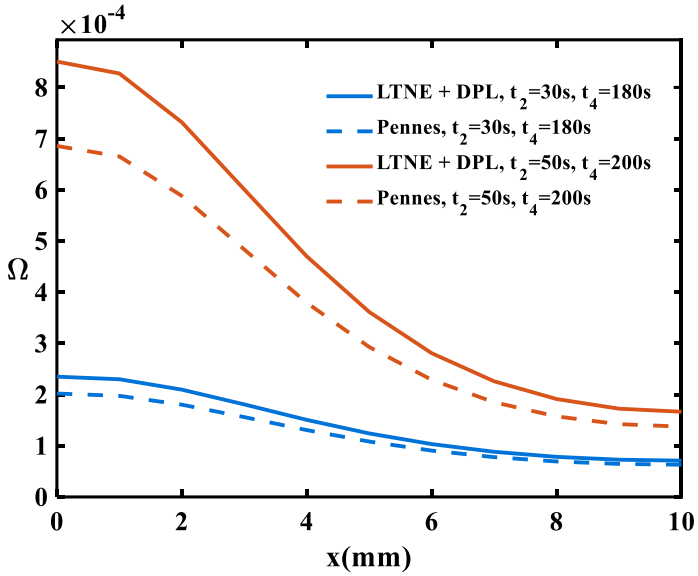


Fig. 15. Variations in the tissue damage parameter along the x-axis for two different laser pulse timing schemes predicted by the Pennes and LTNE+DPL models.

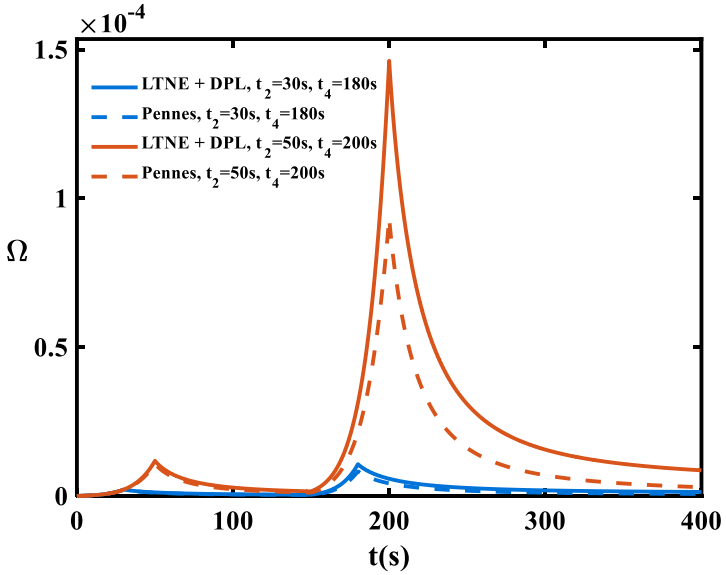


Fig. 16. Temporal variations in the tissue damage parameter for two different laser pulse timing schemes predicted by the Pennes and LTNE+DPL models.

4. Conclusion

In this study, the thermal response of the skin subjected to irradiation by two laser beams was simulated using the LTNE+DPL heat transfer model and compared with that predicted by the classical Pennes model. The results showed that the LTNE+DPL model predicted higher tissue temperatures and greater thermal damage than the Pennes model because it accounts for thermal non-equilibrium between blood and tissue, as well as thermal relaxation effects. It was also found that increasing the laser intensity led to an

increase in the maximum temperature, expansion of the heated region, and an increase in the Arrhenius damage parameter. At an intensity of [value], the maximum temperatures predicted by the LTNE+DPL and Pennes models were 40.16 °C and 39.99 °C, respectively, indicating a temperature difference of 0.166 °C. At 2×10^6 2×10^6 $\frac{W}{m^2}$, these values were 43.27 °C and 42.94 °C, respectively, corresponding to a difference of 0.328 °C. Furthermore, the damage parameter obtained using the LTNE+DPL model was 7% and 16.3% higher than that predicted by the Pennes model, respectively. Therefore, the Pennes model underestimates both temperature and thermal damage compared with the LTNE+DPL model. In addition, changes in pulse timing had a significant effect on the thermal response, with longer pulse application times leading to increased temperature and tissue damage. The temperature distribution along the depth direction showed that the greatest temperature rise occurred in the superficial regions, while temperature and thermal damage decreased with increasing depth because of the attenuation of laser energy absorption. Overall, the results of this study indicate that the LTNE+DPL model can provide more accurate predictions of tissue thermal behavior than the Pennes model and can serve as a useful tool for optimizing laser irradiation parameters and designing safe and effective photothermal treatments.

5. Declarations

The authors declare that they have no known competing financial interests or personal relationships that could have appeared to influence the work reported in this paper.

References

[1] K.-C. Liu, T.-M. Chen, Comparative study of heat transfer and thermal damage assessment models for hyperthermia treatment, Journal of thermal biology, 98 (2021) 102907.

[2] X. Li, X. Tian, The thermal response of three-dimensional skin tissue subjected to multiple laser beams, Waves in Random and Complex Media, 35 (2025) 10440-10455.

[3] A.E. Abouelregal, R.A. Alharb, M. Yaylacı, B.O. Mohamed, S.F. Megahid, Analysis of temperature changes in living tissue using the modified fractional thermal conduction model under laser heat flux on the skin surface, Continuum Mechanics and Thermodynamics, 37 (2025) 13.

[4] N. Stsepuro, P. Nosov, M. Galkin, G. Krasin, M. Kovalev, S. Kudryashov, Generating Bessel-Gaussian beams with controlled axial intensity distribution, Applied Sciences, 10 (2020) 7911.

[5] E. Jawo, M. Hassan, M.M. Almazah, Bio-thermal non-equilibrium dynamics and thermal damage in biological tissues induced by multiple time pulse-laser irradiations, Case Studies in Thermal Engineering, 61 (2024) 104989.

[6] L. Zhang, Y. Wang, Y. Hou, J. Song, Uniform rectangular distribution of far-field intensity by optical phased array, Optics Communications, 507 (2022) 127661.

[7] H.-J. Jiang, Q.-Z. Guo, X.-G. Wang, N.-H. Gao, Analytical solution of three-dimensional temperature field for skin tissue considering blood perfusion rates under laser irradiation and thermal damage analysis, Optik, 312 (2024) 171982.

[8] Y. Wang, X. Lu, W. Zheng, Z. Wang, Bio-thermal response and thermal damage in biological tissues with non-equilibrium effect and temperature-dependent properties induced by pulse-laser irradiation, Journal of Thermal Biology, 113 (2023) 103541.

[9] A. Dinda, J. Acharya, D. Bhanja, S. Nath, Local thermal non-equilibrium bioheat transfer model for interstitial hyperthermia treatment of tumour cell: a numerical approach, Journal of Thermal Biology, 110 (2022) 103368.

[10] M. Jasiński, E. Majchrzak, L. Turchan, Numerical analysis of the interactions between laser and soft tissues using generalized dual-phase lag equation, Applied Mathematical Modelling, 40 (2016) 750-762.

[11] F. Hamzavi, M.J. Karimi, M. Bahadoran, Numerical analysis of microwave and radiofrequency ablations: A novel design for electrode-based radiofrequency ablation, Journal of Thermal Biology, (2025) 104247.

[12] B. Shariati BK, M.A. Ansari, S.S. Khatami, V.V. Tuchin, Multimodal optical clearing to minimize light attenuation in biological tissues, Scientific Reports, 13 (2023) 21509.

[13] L. Kaub, C. Schmitz, Comparison of the penetration depth of 905 nm and 1064 nm laser light in surface layers of biological tissue ex vivo, Biomedicines, 11 (2023) 1355.

[14] M. Singh, T. Singh, S. Soni, Pre-operative assessment of ablation margins for variable blood perfusion metrics in a magnetic resonance imaging based complex breast tumour anatomy: Simulation paradigms in thermal therapies, Computer Methods and Programs in Biomedicine, 198 (2021) 105781.

[15] R. Shi, L. Xia, Y. Ding, Y. Yu, Z. Wang, Y. Ma, Study on temperature variation characteristics of biological skin tissue irradiated by 1064 nm long-and Short-Pulse lasers, Optics & Laser Technology, 203 (2026) 115861.